Available online at www.sciencedirect.com

ScienceDirect

journal homepage: http://www.elsevier.com/locate/acme

Original Research Article

Investigation of the effective elastic parameters in the discrete element model of granular material by the triaxial compression test

I. Marczewska [a,*], J. Rojek [a], R. Kačianauskas [b]

[a] Institute of Fundamental Technological Research, Polish Academy of Sciences, Pawińskiego 5B, 02-106 Warsaw, Poland[1]

[b] Vilnius Gediminas Technical University, Sauletekio al. 11, 10223 Vilnius, Lithuania

ARTICLE INFO

Article history:
Received 15 March 2015
Accepted 27 September 2015
Available online 26 October 2015

Keywords:
Discrete element method
Granular material
Triaxial test
Micro–macro relationship
Voigt hypothesis

ABSTRACT

The general objective of the present paper is to improve the understanding of micromechanical mechanisms in granular materials and their representation in numerical models. Results of numerical investigations on micro–macro relationships in the discrete element model of granular material are presented. The macroscopic response is analysed in a series of simulations of the triaxial compression test. The numerical studies are focused on the influence of microscopic parameters on the initial response. The effect of the contact stiffness and friction coefficient on the effective elastic moduli is investigated. Numerical results are compared with the analytical estimations based on the kinematic Voigt's hypothesis as well as with selected numerical results of other authors. The comparisons show that a better agreement between the numerical and analytical results is observed for particle assemblies with higher coordination numbers. Higher coordination numbers are related to more compact specimens and for a given specimen can be associated with low values of the contact stiffness and a higher confining pressure.

1. Introduction

The discrete element method (DEM) proposed by Cundall and Strack [1] is a numerical procedure, in which a material is represented as a large assembly of rigid particles (discrete elements) interacting with each other by contact forces. It is a suitable tool to model materials with discontinuities. It has become a very popular framework to model granular materials in many applications in areas such as soil mechanics [2,3], geotechnics [4,5], agriculture [6,7], powder metallurgy [8] and others [9]. The DEM can also be used to model cohesive materials such as rocks [10,11] and concrete [12].

The discrete elements can be of spherical, e.g. [2,3,6], or non-spherical, e.g. [13,14], shape. In the present work, the spherical particles are used. The spherical geometry of the

[1] Tel.: +48 22 8261281.
[*] *Corresponding author.*
E-mail address: imar@ippt.gov.pl (I. Marczewska).

http://dx.doi.org/10.1016/j.acme.2015.09.010

particle is idealized and does not accurately model phenomena exhibited by a real granular material. It has been shown that spherical particles give a smaller angle of repose and reduced shear strength as compared to non-spherical particles [13]. This is due to the fact that the rotation is only resisted by frictional contacts with neighbouring particles; whereas for non-spherical particles, the rotation tends to be inhibited by mechanical interlocking. The deficiencies of spherical particles can be mitigated to a certain degree by introducing the rotational friction in the contact model. It has been shown in [9], that the rotational friction increases the angle of repose. Including the rolling friction allows to reproduce properly macroscopic flow of a granular material [6]. Despite their deficiencies spherical particles are very popular in the DEM, e.g. [2,3], and are very often chosen for simulation mainly because of their low computational costs.

The discrete element model is a micromechanical material model. A required macroscopic behaviour is obtained taking an adequate contact model with appropriate parameters. The macroscopic response of a granular material is described by the deformability, strength, dilatancy, strain localization etc. The initial deformation is characterized by the elastic constants, i.e. Young's modulus, Poisson's ratio, bulk modulus and shear modulus. The discrete element model is defined in terms of microscopic parameters such as the interparticle contact stiffness parameters, damping coefficients, rolling and sliding friction. A simple contact model employing a linear law for the normal compressive force and the frictional Coulomb model for the tangential force has been used in this work.

Use of the discrete element model requires determination of the microscopic contact parameters. It is sometimes possible to measure material and contact properties of a single particle [6,7], but in most cases macroscopic tests and measurements on a granular material are available only. Then in order to determine the microscopic parameters the relationships between microscopic and macroscopic parameters must be established. Constitutive micro–macro relationships for discrete element models of granular materials can be obtained analytically or numerically.

In analytical approaches, based on micromechanical modelling and homogenization procedures, effective macroscopic properties are derived in terms of interparticle parameters and particle assembly properties, cf. [15–18]. Theoretical micromechanical approaches employ the kinematic hypothesis of uniform strain (Voigt's hypothesis), cf. [15–17] or the static hypothesis of uniform stress (Reuss hypothesis), cf. [19]. The Voigt's kinematic hypothesis leads to an upper bound solution for elastic moduli. Implementation of the static hypothesis for granular materials does not often strictly satisfy all the requirements of equilibrium and therefore lower estimation and not lower bound solution can be obtained, cf. [19].

Different simplifying assumptions are required in the microstructural analysis. Many formulations assume equal size particle assembly, cf. [20,21] or regular particle configuration, cf. [22–24]. Some of the above referenced works, cf. [15–17] employ the assumption that there is no sliding at contacts, thus they are applicable to small strain and elastic behaviour only. The microstructural constitutive relationship for granular systems has been extended in [25] to take into account the effect of particle separation and sliding under large deformation. The extension consisted in applying a standard homogenization procedure in an incremental way to a statistical representation of a granular material.

Numerical simulations are a useful tool to study micromechanical mechanisms in granular materials. Numerical investigation of elastic properties of granular packings has been presented in [26]. Micromechanical study of elastic moduli of two-dimensional granular assemblies using the DEM has also been carried out in [27,23]. Theoretical micromechanical predictions of effective moduli of identical spheres have been compared with numerical simulations in [21]. Comparisons of numerical and theoretical results show that in some cases, analytical estimation gives good results, cf. [23], but in many cases, discrepancy between analytical estimations and numerical results can be observed, cf. [28]. The discrepancy is caused by the lack of compatibility of the discrete element assembly characteristics with the simplifying assumptions of the theoretical homogenization. Therefore, analytical equations can be used for a preliminary estimation of the microscopic parameters, but numerical simulations are necessary in a more reliable calibration of the discrete element model.

The numerical calibration of a discrete element model of granular materials can be performed employing the computational homogenization approach [29,12] or by simulation of laboratory tests, such as the direct shear test [5,30,31], the repose angle test [9], or the triaxial compression test [3,32,33]. Microscopic parameters are determined by fitting numerical result to experimental one. A discrete element model of the triaxial compression test will be used in the numerical studies in the present work.

The investigation is focused on the initial response and elastic effective moduli of a granular material. The term ''elastic'' is used here in the sense adopted in an engineering practice for moduli measured in standard laboratory tests. Actually, the tangent moduli obtained from the slopes of respective experimental stress–strain curves are not ''true elastic'' since they are influenced not only by the elasticity of the material but also by irreversible effects caused by the friction and grain rearrangement [26].

The present work has been aimed to establish the relationships between the microscopic parameters and macroscopic properties of a granular material and to verify validity of the theoretical formulae for elastic moduli for a wide range of microscopic parameters influencing the elastic response. We have tried to fill the gap between the works aiming just to calibrate the model by matching numerical results to experimental ones and the works presenting micromechanical studies.

The elastic moduli obtained in numerical simulations will be compared with analytical estimations according to the Voigt's hypothesis. The closed-form expressions for the Voigt's bounds are obtained assuming only force interactions therefore in our simulations we will use the contact model taking into account the force interaction only, and neglecting the moment interaction due to the rolling friction. We are aware that by neglecting the rolling friction we impose some limitations on the range of possible macroscopic parameters [34], nevertheless, it is necessary to understand micromechanical mechanisms of this simple model before enriching it with other effects such as the moment interactions.

2. Discrete element method formulation

Numerical simulations have been performed using the discrete element code DEMPack [35]. The discrete element algorithm implemented in this program is presented in a number of publications [9,36,37]. Here, the formulation of the contact model for granular materials will be presented shortly.

Let us consider a pair of contacting particles, i and j, with the radii r_i and r_j, shown in Fig. 1. The positions of the particle centroids in the inertial coordinate system are given by the vectors $\mathbf{x}_i$ and $\mathbf{x}_j$. The motion of the particles is described by the translational velocities of the centroids $\mathbf{v}_i$ and $\mathbf{v}_j$, and the rotational velocities $\boldsymbol{\omega}_i$ and $\boldsymbol{\omega}_j$.

The interaction of the particles is described by the frictional contact model. The normal contact force F_n is composed of the elastic part F_{ne} and the damping component F_{nd}

$$F_n = F_{ne} + F_{nd}. \tag{1}$$

The elastic force F_{ne} is given by the linear relationship

$$F_{ne} = k_n u_{rn}, \tag{2}$$

where k_n is the normal contact stiffness and u_{rn} is the overlap of the two particles. The particle overlap u_{rn} is given in terms of the distance between the particle centroids d_{ij} and their radii r_i and r_j

$$u_{rn} = d_{ij} - r_i - r_j, \tag{3}$$

where

$$d_{ij} = \|\mathbf{x}_i - \mathbf{x}_j\|. \tag{4}$$

The two particles are in contact if $u_{rn} \le 0$.

The damping force, which is introduced to dissipate kinetic energy and to decrease oscillations of the contact forces, is assumed to be of viscous type

$$F_{nd} = c_n v_{rn} \tag{5}$$

where v_{rn} is the normal relative velocity of the centres of the two particles in contact and c_n is the damping coefficient. The damping coefficient can be taken as an appropriate fraction ζ_n of the critical damping c_n^{cr}

$$c_n = \zeta_n c_n^{cr} \tag{6}$$

For the system of two rigid spheres with masses m_i and m_j connected with a spring of stiffness k_n, the critical damping is given by the following expression:

$$c_n^{cr} = 2\sqrt{\frac{m_i m_j k_n}{m_i + m_j}} \tag{7}$$

The tangential reaction $\mathbf{F}_t$ is brought about by friction opposing the relative motion at the contact point. The friction is considered assuming the regularized Coulomb model with the tangential contact stiffness k_t and friction coefficient μ as the model parameters. The tangential contact force is calculated in an incremental way

$$\Delta\mathbf{F}_t = -k_t \mathbf{v}_{rt} \Delta t, \tag{8}$$

where $\mathbf{v}_{rt}$ is the tangential component of the relative velocity at the contact point. The slip/stick condition

$$\phi = \|\mathbf{F}_t\| - \mu|F_n| \le 0 \tag{9}$$

is checked for the tangential force. If evaluation given by Eq. (9) yields $\phi > 0$ the radial return algorithm analogous to that used in elastoplasticity is used to ensure satisfaction of condition (9).

The elastic properties of the micromechanical (contact) model are defined by the normal and tangential contact stiffness, k_n and k_t. We can distinguish two approaches in evaluation of these parameters [37]. In the first approach, these parameters are calculated locally as a function of a material property and the contacting particle size [11,37], while in the other approach the parameters k_n and k_t are taken as uniform in the whole discrete element assembly [10]. In the present study, the latter approach has been used since it is compatible with the assumptions used to obtain closed-form formulae in theoretical homogenization.

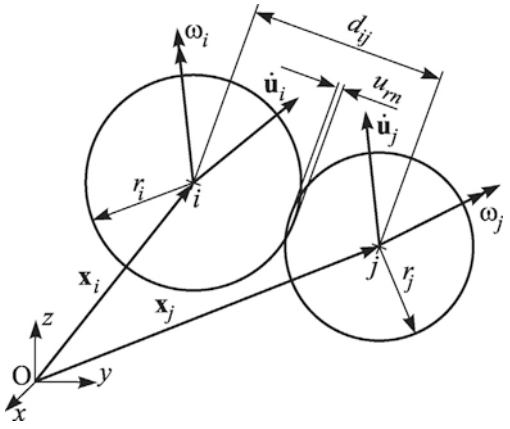

Fig. 1 – Definition of geometrical and kinematical parameters in the contact of two particles.

3. Analytical micro–macro relationships

The numerical results will be compared with analytical micro–macro relationships derived from the Voigt's kinematic hypothesis which is commonly used in homogenization procedures. Traditional homogenization methods were developed for estimation of effective properties of heterogenous materials. The Voigt's hypothesis is based on the assumption of uniform strain which introduces a kinematic constraint leading to a stiffer behaviour than that of a real material without a constraint. Therefore the Voigt's theory predicts upper bounds for elastic moduli.

When the Voigt's theory is applied to a granular material represented by a particle assembly it is assumed that the displacements of individual particles are in accordance with the displacement field induced by the uniform strain ε_{ij}. This allows us to express the relative displacement u_i^c of a pair of contacting particles as:

$$u_i^c = \varepsilon_{ij} L_j^c \tag{10}$$

where L_j^c is the so called branch vector – vector connecting particle centroids. Assuming that particles are rigid and discontinuities are localized at the contact point the vector u_i^c is equivalent to the relative displacement at the contact point, so the local constitutive law can be written as

$$F_i^c = K_{ij}^c u_j^c \tag{11}$$

where F_i^c is the contact force, and K_{ij}^c is the contact stiffness tensor, which can be expressed in terms of the normal and tangential stiffness as follows:

$$K_{ij} = k_n n_i n_j + k_t(s_i s_j + t_i t_j) \tag{12}$$

where n_i is the unit normal vector at the contact, and s_i and t_i arbitrary orthogonal tangent unit vectors. Using Eqs. (10) and (11) together with the expression for averaged stresses, cf. [19]:

$$\sigma_{ij} = \frac{1}{V}\sum_c L_i^c F_j^c \tag{13}$$

where V is the averaging volume, and assuming the average stress–strain relationship

$$\sigma_{ij} = C_{ijkl}\varepsilon_{ij} \tag{14}$$

the following constitutive tensor can be derived, cf. [19]:

$$C_{ijkl} = \frac{1}{V}\sum_c L_i^c K_{jk}^c L_l^c \tag{15}$$

For the assembly of spherical particles of the same size and same material properties with isotropic packing structure the closed-form formulae for the stress-strain relationship of Eq. (14) can be derived. Then, the equivalent macroscopic constitutive tensor C_{ijkl} can be expressed in terms of the elastic moduli: the Young's modulus E, the Poisson's ratio ν, the bulk modulus K or the shear modulus G of the following form [19,38]:

$$E = \frac{4N_c r^2 k_n}{3V}\cdot\frac{2k_n + 3k_t}{4k_n + k_t} \tag{16}$$

$$\nu = \frac{k_n - k_t}{4k_n + k_t} \tag{17}$$

$$K = \frac{4N_c r^2}{9V}k_n \tag{18}$$

$$G = \frac{4N_c r^2 k_n}{3V}\cdot\frac{2k_n + 3k_t}{10k_n} \tag{19}$$

where N_c is the total number of inter-particle contacts in the volume V, r is the particle radius, k_n and k_t are the contact stiffness in the normal and tangential direction, respectively.

Expressing the specimen volume V in terms of the particle volumes V_p and specimen porosity e

$$V = \frac{N_p V_p}{1-e} \tag{20}$$

where N_p is the number of particles and

$$V_p = \frac{4}{3}\pi r^3 \tag{21}$$

we can present the above Eqs. (16), (18) and (19) for the macroscopic moduli E, K and G in the following form:

$$E = \frac{n_c(1-e)k_n}{2\pi r}\cdot\frac{2k_n + 3k_t}{4k_n + k_t} \tag{22}$$

$$K = \frac{n_c(1-e)}{6\pi r}k_n \tag{23}$$

$$G = \frac{n_c(1-e)k_n}{2\pi r}\cdot\frac{2k_n + 3k_t}{10k_n} \tag{24}$$

where n_c is the so called coordination number, a parameter defined as an average number of contacts per particle

$$n_c = \frac{2N_c}{N_p} \tag{25}$$

The above equations are valid for the stick contact without sliding and without any moment interaction at the contact point. They have been derived assuming equal size of the particles. Applying Eqs. (22)–(24) for an assembly of different size particles we will use the average (arithmetic mean) of all the particle radii as the parameter r. Averaging will be performed over the whole volume of the numerical specimen.

4. Numerical results

4.1. *Discrete element model*

Micro–macro relationships for elastic parameters have been obtained by simulation of the triaxial compression test which is a standard laboratory test procedure widely used to measure mechanical properties of soils and other granular materials [4]. The numerical simulations have been performed using the

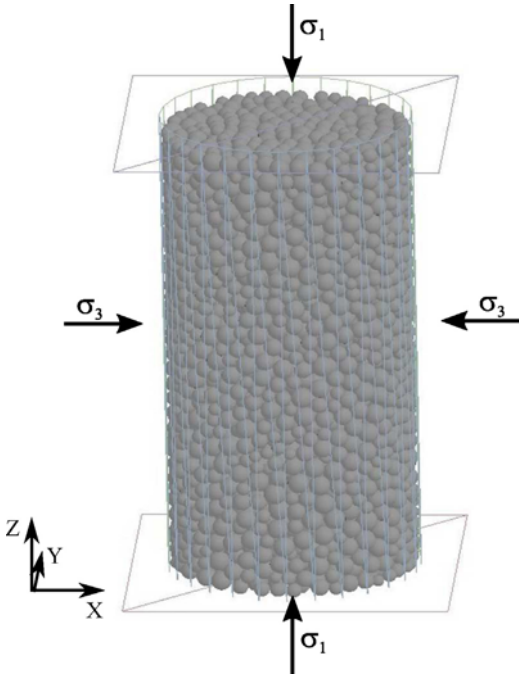

Fig. 2 – Discrete element model of the triaxial compression tests.

specimen shown in Fig. 2. The specimen is composed of 5,430 spherical particles with radii varying from $r_{min} = 0.0462$ cm to $r_{max} = 0.089$ cm (the average radius $r = 0.0677$ cm) confined within a cylinder with a diameter $D = 2R = 2$ cm and a height $H = 4$ cm. The specimen has been generated using the high density sphere packing algorithm based on the optimization procedure with geometrical constraints developed in [39].

The sample H/D ratio is similar to that used in laboratory experiments. The initial porosity of the specimen is $e = 0.39$. The particle mass density was equal to $\rho = 1660$ kg/m^3. Gravity has not been considered. The interparticle Coulomb friction coefficient $\mu = 0.577$ has been assumed. The confining rigid walls have been assumed as nearly smooth with the Coulomb coefficient $\mu = 0.02$ for the particle–wall friction. The top and bottom plate motion is independent of each other and of the sidewall motion. The cylinder sidewall has been assumed to shrink or expand uniformly. The loading has been introduced in two stages. In the first stage, the specimen has been compressed by the hydrostatic pressure σ_3. In the second stage, the axial strain has been increased monotonically while keeping the pressure on the lateral walls constant. The axial compressive strain has been introduced moving the upper and lower walls with a constant velocity 0.01 m/s along the axial direction. The low loading velocity and an appropriate damping have guaranteed a quasi-static character of the dynamic process. The damping used in the analysis has been evaluated taking the coefficient $\zeta_n = 0.7$ in Eq. (6).

The macroscopic behaviour of the granular material modelled with spherical particles has been studied for different values of micromechanical parameters: the contact stiffness k_n and the ratio of the contact stiffness in the tangential and normal directions k_t/k_n. The response of the granular material was characterized in terms of the confining pressure σ_3, axial stress σ_1, deviatoric stress q, axial, radial and volumetric strains, ε_a, ε_r and ε_V, respectively. The deviatoric stress q is defined as:

$$q = \sigma_1 - \sigma_3 \tag{26}$$

The axial strain ε_a has been calculated as:

$$\varepsilon_a = \frac{\Delta H}{H} \tag{27}$$

where ΔH is the change of the height and H is the original height of the specimen. The volumetric strain has been obtained from the relationship:

$$\varepsilon_V = \varepsilon_a + 2\varepsilon_r \tag{28}$$

The elastic macroscopic parameters, the Young's modulus E and the Poisson's ratio ν, have been determined from the initial slopes of the deviatoric stress vs. axial strain and volumetric strain vs. axial strain curves using the following equation

$$E = \frac{dq}{d\varepsilon_a} \tag{29}$$

$$\nu = \frac{(d\varepsilon_V/d\varepsilon_a) + 1}{2} \tag{30}$$

The two other elastic moduli, the bulk and shear moduli, K and G, respectively, can be calculated from the well known equation:

$$K = \frac{E}{3(1-2\nu)} \tag{31}$$

$$G = \frac{E}{2(1+\nu)} \tag{32}$$

4.2. *Effect of the contact stiffness on the material response*

In order to investigate the influence of the contact stiffness on the macroscopic response a number of simulations have been performed changing the contact stiffness k_n in the range from 9×10^3 to 7.5×10^6 N/m, keeping the ratio k_t/k_n constant and equal to 0.35, and assuming a confining pressure of 100 kPa. The time integration was carried out using the step ranging from 5.2×10^{-8} s (for $k_n = 7.5 \times 10^6$ N/m) to 1.5×10^{-6} s (for $k_n = 9 \times 10^3$ N/m). The numerical results are shown in Figs. 3 and 4 in the form of the curves indicating the evolution of the deviatoric stress and volumetric strain, respectively, as functions of the axial strain, for different values of the contact stiffness in the normal direction k_n.

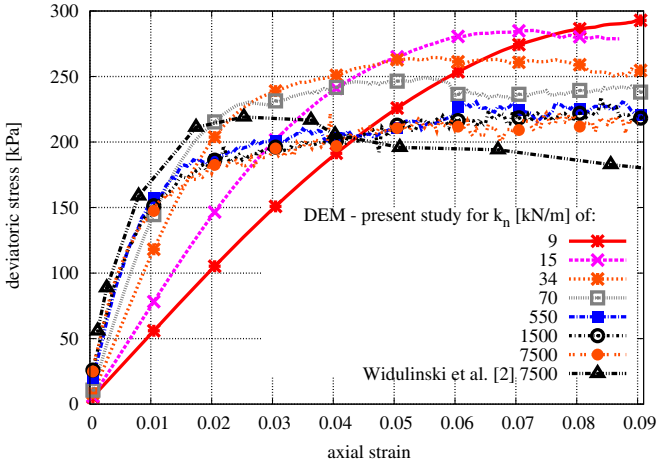

Fig. 3 – Evolution of the deviatoric stress as a function of the axial strain for different values of the contact stiffness in the normal direction.

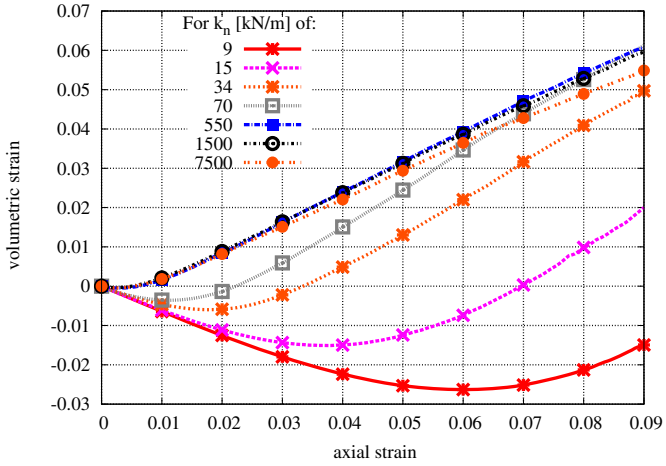

Fig. 4 – Evolution of the volumetric strain as a function of the axial strain for different values of the contact stiffness in the normal direction.

It can be seen in Fig. 3, that the slope of the stress–strain curves equal to the Young's modulus increases with an increase of the contact stiffness, however, the effect of the contact stiffness on the initial slope of the stress–strain curve for higher values of the contact stiffness is very small, which is in agreement with observations of other researchers, cf. [40]. The results obtained in the present work are confronted in Fig. 3 with the results obtained in [2] with the contact stiffness $k_n = 7500$ kN/m and the ratio $k_t/k_n = 0.3$. Some of the characteristics of the specimen used in [2] (particle radius range 0.2–0.8 mm, the average radius 0.5 mm, porosity $e = 0.375$ and Coulomb friction coefficient $\mu = 0.524$) are similar to that used in the present work, nevertheless particle size distribution may be different in both specimens. Despite this, Fig. 3 shows that the curve from [2] is similar to the curves obtained in this work for a high contact stiffness.

The contact stiffness has also a large influence on the volumetric strain as it is shown in Fig. 4. The curves of the volumetric strain versus axial strain, indicate an initial decrease of the specimen volume (contraction) until a certain value of the axial strain at which the contraction–dilatancy transition can be observed. With an increase of the contact stiffness the contraction phase gets shorter. Similarly as in the case of the stress–curves we can observe that when the contact stiffness reaches a certain threshold, further increase of the contact stiffness has no effect on the volumetric response.

The effect of the contact stiffness on the stress and strain response of the discrete element assembly can be understood analysing influence of the contact stiffness on the interparticle forces and relative motion [41]. The global deformation of the particle assembly results from the change of the amount of particle overlapping and particle rearrangement. Particle overlapping represents deformation of the grains in a real material. In the initial phase of the triaxial test (contraction phase), the change of the volume is mainly due to the particle deformation and the small relative motion due to the sliding friction. In the second phase of the test (dilatancy phase) mutual particle rearrangement dominates over the deformation of particles. Similar mechanisms are reproduced in the discrete element simulation. In the initial phase, the elastic deformation dominates, the particle overlapping increases under an increasing normal force and the small tangential relative motion occurs under the stick conditions of the friction model. The particle rearrangement starts to play a major role when the friction force exceeds the stick limit and the slip regime develops. This rearrangement has a local character and leads initially to a densification of the material, cf. [8]. When the process goes further the large particle mutual rolling and sliding increase rearrangement of the particles, leading to the increase of the volume (dilatancy) of the whole assembly. The higher the contact stiffness the smaller is the overlap between the particles and its contribution to the overall deformation of the particle assembly. The sliding regime and particle rearrangement develop faster therefore the contraction phase is shorter.

The processes at the micromechanical level are reflected in the evolution of coordination number (average number of contacts per particle) n_c plotted in Fig. 5. Densification of the granular matter in the initial phase is associated with an

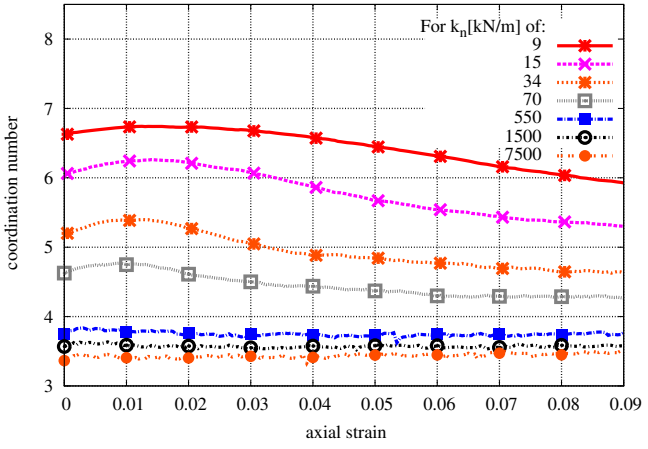

Fig. 5 – Evolution of the coordination number n_c for different values of the contact stiffness in the normal direction.

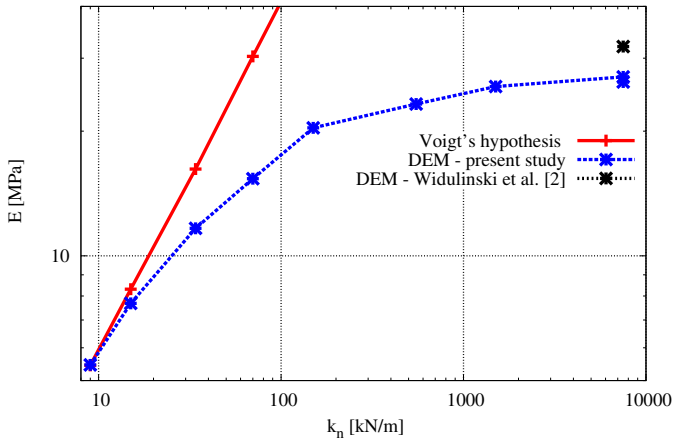

Fig. 6 – Dependence of the Young's modulus on the normal contact stiffness.

increase of the coordination number. During the dilatancy phase when the granular material becomes looser the number of contacts decreases. The number of contacts depends on the contact stiffness. The lower the contact stiffness the larger overlap of the particles is allowed and the larger is the number of contacts in the assembly. In case of high stiffness the contact of particles can be less stable – the particles can lose contact due to local oscillations.

Dependence of the Young's modulus E on the contact stiffness k_n obtained in the numerical simulations is plotted in Fig. 6. Numerical results are compared with the analytical upper limit calculated from Eq. (16). It can be seen that the numerical estimations of the Young's modulus agree quite well with the analytical predictions for lower values of the contact stiffness. As the contact stiffness increases the numerical estimations of the Young's modulus diverge from the analytical bound. The numerical results obtained in the present work are consistent with the result from [2]. The analysis performed by Widuliński et al. [2] was a part of the calibration of the DEM model to match experimental data of a sand. The results obtained in this work make up a bridge between the range of the contact stiffness in which the analytical estimations are valid and the range of the contact stiffness required to match macroscopic properties of such materials as a sand.

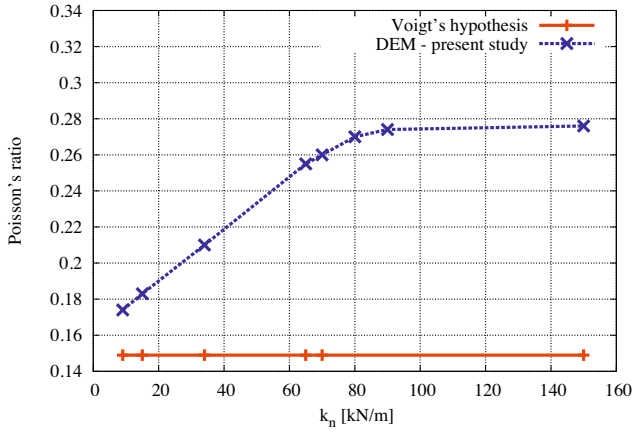

Fig. 7 – Poisson's ratio from DEM simulations and estimated by Voigt's hypothesis as functions of the normal contact stiffness.

Numerical and theoretical dependence of the Poisson's ratio on the contact stiffness k_n is shown in Fig. 7. The Voigt's hypothesis provides a lower bound estimation of the Poisson's ratio given by Eq. (17). Similarly as for the Young's modulus, the agreement between numerical and analytical results is quite good for the lower values of the contact stiffness and worse for the higher values.

4.3. *Effect of the stiffness ratio on material response*

Let us rewrite the analytical expressions for the elastic constants given by Eqs. (17) and (22)–(24) as follows:

$$\frac{2\pi E r}{n_c(1-e)k_n} = \frac{2+3(k_t/k_n)}{4+(k_t/k_n)} \tag{33}$$

$$\nu = \frac{1-(k_t/k_n)}{4+(k_t/k_n)} \tag{34}$$

$$\frac{6\pi K r}{n_c(1-e)k_n} = 1 \tag{35}$$

$$\frac{2\pi G r}{n_c(1-e)k_n} = \frac{2+3(k_t/k_n)}{10} \tag{36}$$

In this way, we have obtained the dimensionless relationships being the functions of the stiffness ratio k_t/k_n.

Until now, the simulations were performed keeping the ratio k_t/k_n constant. The theoretical formulae given by Eqs. (33) and (34) show that the elastic macroscopic constants E and ν should depend on the ratio k_t/k_n, while the relationship (35) indicates that the bulk modulus K should be independent of the ratio k_t/k_n. The effect of the ratio k_t/k_n on the elastic constants E, ν, K and G have been investigated numerically. The numerical studies have been performed taking the confining pressure of 100 kPa for 3 cases of the contact stiffness in the normal direction $k_n = 9$, 15 and 34 kN/m and changing the ratio k_t/k_n in the interval 0.04–1.0.

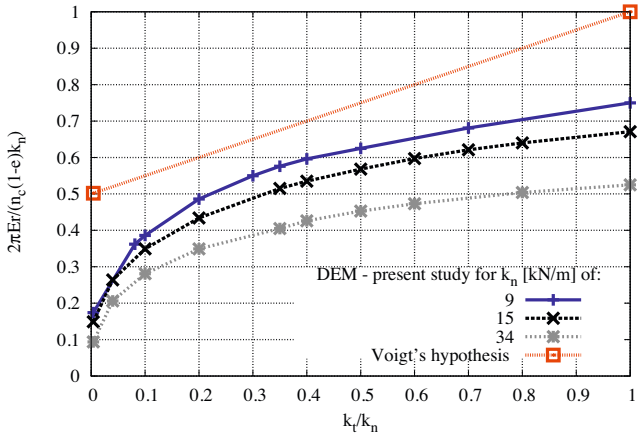

Fig. 8 – Analytical and numerical dimensionless relationships involving the Young's modulus as functions of the ratio k_t/k_n.

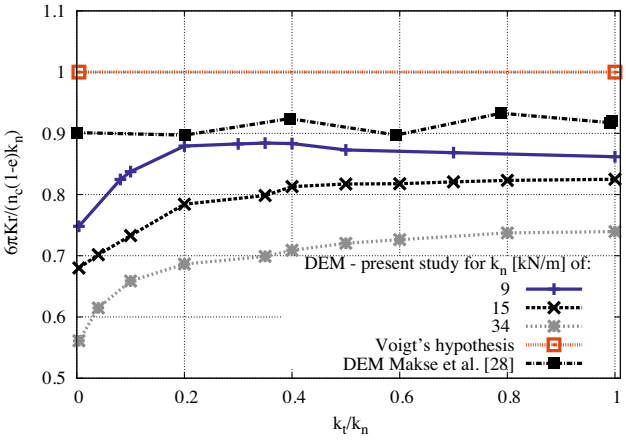

Fig. 10 – Analytical and numerical dimensionless relationships involving the bulk modulus as functions of the ratio k_t/k_n.

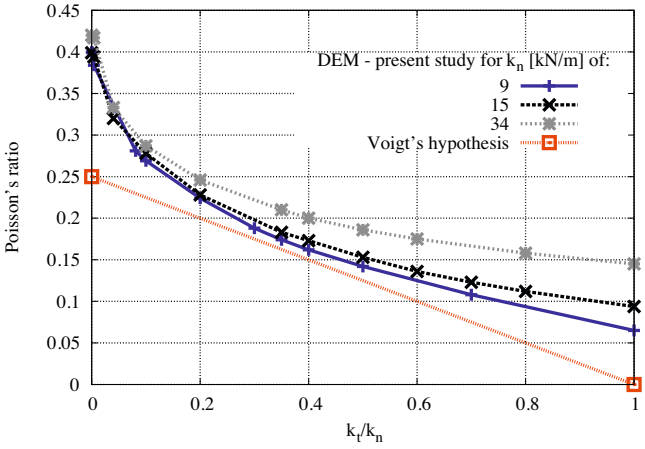

Fig. 9 – Poisson's ratio as a function of the ratio k_t/k_n – comparison of numerical and analytical relationships.

Influence of the ratio k_t/k_n on the macroscopic elastic moduli is shown in the form of a dimensionless relationships in Figs. 8–11. The dimensionless parameters involving the Young's modulus E, Poisson's ratio ν, the bulk modulus K and the shear modulus G are defined by the left-hand sides of Eqs. (33)–(36). The right-hand sides of Eqs. (33)–(36) provide theoretical predictions plotted in Figs. 8–11. The results plotted in Figs. 10 and 11 also include the results given in [28].

In Figs. (8)–(11), it can be seen that the numerical results are bounded by the theoretical predictions derived using the Voigt's hypothesis. The lower the contact stiffness k_n, the closer are the numerical results to the theoretical ones, which is in agreement with our previous observations. The numerical curves for the parameters involving the Young's modulus, Poisson's ratio and shear modulus, agree better with the theoretical estimations for a range of the ratio k_t/k_n from 0.2 to 0.5 approximately and diverge more when the value of the ratio k_t/k_n is close to 0 or 1.

The contact stiffness is inversely correlated with the average coordination number. This, combined with the former

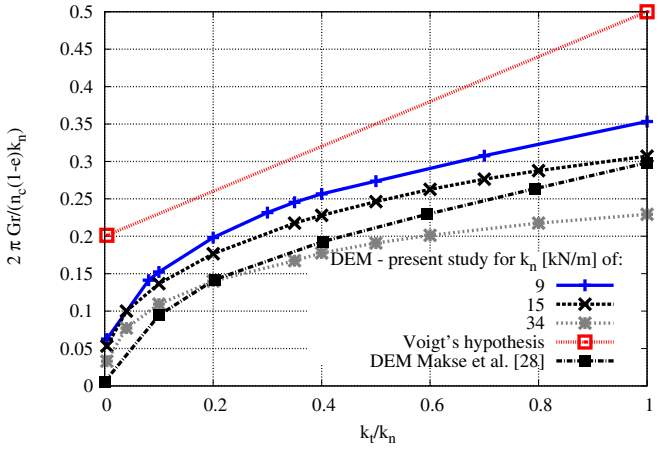

Fig. 11 – Analytical and numerical dimensionless relationships involving the shear modulus as functions of the ratio k_t/k_n.

observation, allows us to notice that the theoretical predictions based on the Voigt's hypothesis are less accurate for assemblies with lower coordination numbers. A similar conclusion, for the 2D DEM model, is presented by Kruyt et al. [23], where the authors notice that the deviations of the numerical results from the theoretical predictions decrease with increasing coordination number.

According to the theoretical predictions given by Eqs. (18) and (23), the bulk modulus should be independent of the stiffness ratio. The numerical simulations give almost constant value of the dimensionless parameter, involving the bulk modulus relatively close to the theoretical value, in most of the studied intervals of the stiffness ratio (see Fig. 10). However, the numerical curves show a strong dependence of the bulk modulus on the stiffness ratio k_t/k_n, when this ratio is close to zero, which agrees with the observations for a 2D DEM model presented by Kruyt et al. [23]. This effect is not observed in the numerical results from [28] plotted in Fig. 10. A good qualitative agreement between our numerical results and the results from [28] can be observed for the curves plotted in Fig. 11 showing the dependence of the shear modulus on the stiffness ratio. A more detailed quantitative comparison of our results with those from [28] are difficult since the normal contact in our simulations is described by the linear relationship (2) and the Hertz model is used in [28].

It should be remarked that the dimensionless numbers defined by the left hand sides of Eqs. (33)–(36) constitute an original element of the present work. They allow us to analyse assemblies with different coordination numbers and porosities in one diagram. Other authors, cf. [23], do not include the coordination number in the definition of the dimensionless number, which make it necessary to analyse assemblies with different contact stiffness separately.

4.3.1. *Effect of the Coulomb friction coefficient on material response*

The analytical formulae for the macroscopic elastic moduli given by Eqs. (16)–(19) are based on the assumption that there is no sliding at the contact points. It is not easy or even impossible to satisfy this requirement in a cohesionless discrete element model of a granular material. As it was discussed in Section 4.2 sliding occurs from an early stage of loading and influences material response in the range considered as elastic. The sliding mode of friction is governed by the Coulomb friction coefficient. This parameter should be considered in parametric studies of discrete element models [2,42]. Widuliński et al. [2] have investigated the effect of the friction coefficient on the peak and residual stress and the dilatancy angle in the triaxial compression test. Role of interparticle friction in the shear-strength mechanism of granular material has been investigated in [42]. The numerical studies in this work are focused on an effect of this parameter on an initial material response.

Numerical studies have been performed taking the confining pressure of 100 kPa, the normal stiffness k_n = 15 kN/m and the stiffness ratio k_t/k_n = 0.35. The Coulomb friction coefficient has been assumed to vary in the intervals of 0.01–0.6. The values of the stiffness and stiffness ratio assumed for the sensitivity studies in the present and following sections

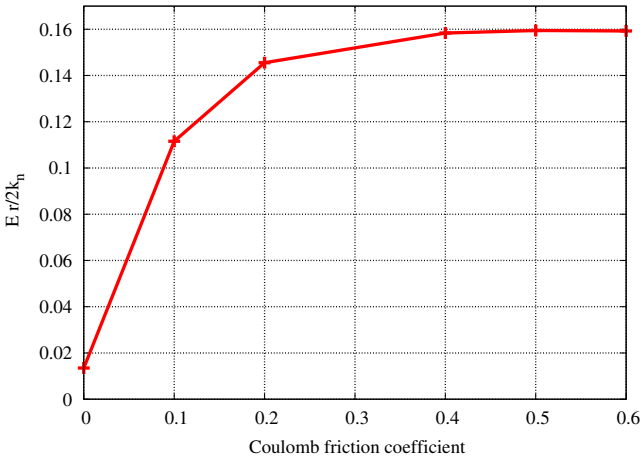

Fig. 12 – Dimensionless dependency between the macroscopic Young's modulus and microscopic Coulomb friction coefficients.

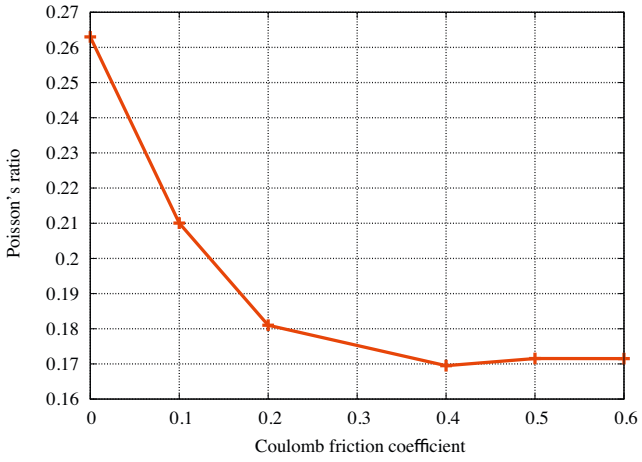

Fig. 13 – Dependence of the Poisson's ratio on the Coulomb friction coefficient.

yielded the elastic moduli relatively close to the analytical predictions in the simulations reported in Figs. 8–11.

Dependency of the elastic macroscopic properties, the Young's modulus and Poisson's ratio, on the Coulomb friction coefficient is presented in the dimensionless form in Figs. 12 and 13. The curve plotted in Fig. 12 shows that initially the Young's modulus increases with an increase of the friction coefficient, but it stabilizes when the friction coefficient exceeds the value of 0.4. The Poisson's ratio plotted in Fig. 13, decreases when the friction increases from 0.01 to 0.4, and stabilizes for higher values of the friction coefficients. Independence of the elastic moduli of the friction coefficient for its values larger than a certain threshold can be explained by the fact that for the higher values of the friction coefficients most of friction forces are below the slip limit and the friction occurs in the stick mode (in the elastic range).

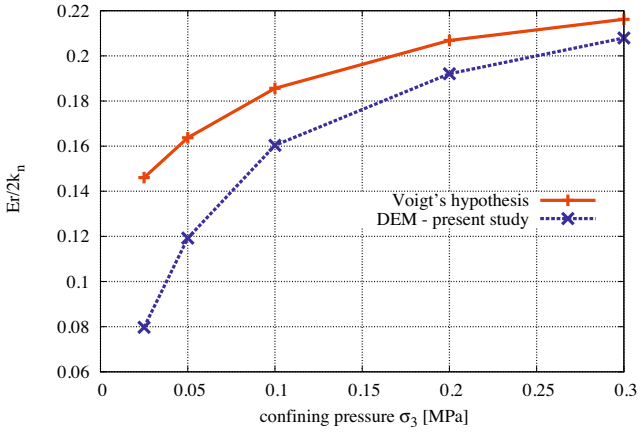

Fig. 14 – Dimensionless relationship between the Young's modulus and confining pressure.

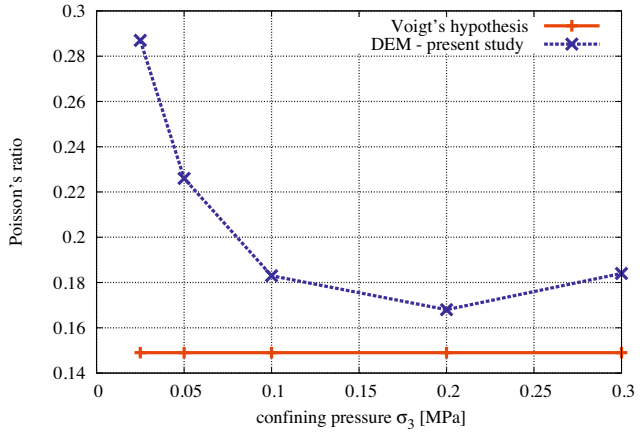

Fig. 15 – Relationship between the Poisson's ratio and the confining pressure.

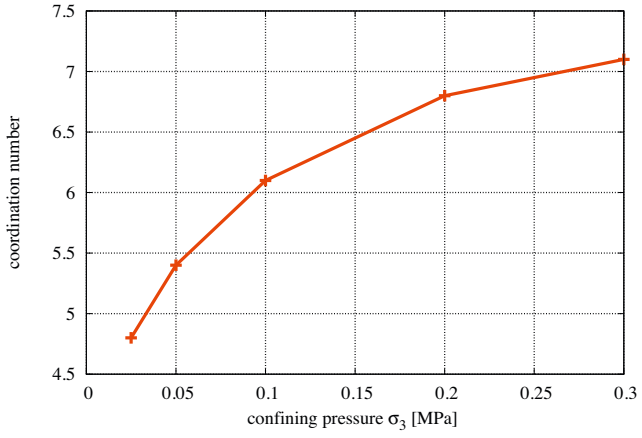

Fig. 16 – Dependence of the coordination number on the confining pressure.

4.3.2. *Effect of the confining pressure on the material response*
The laboratory triaxial compression test is performed for a range of confining pressure which could exist in in-situ conditions. This enables determination of the strength envelope of material. Here, an attention has been focused on the influence of the confining pressure on the initial response, and the elastic moduli of granular material modelled with the discrete element method.

The numerical studies have been performed taking the confining pressure of 25, 50, 100, 200 and 300 kPa, taking the normal stiffness $k_n = 15$ kN/m, the stiffness ratio $k_t/k_n = 0.35$ and the Coulomb friction coefficient $\mu = 0.577$. The numerical and theoretical results showing the effect of the confining pressure on the Young's modulus and Poisson's ratio, are plotted in Figs. 14 and 15, respectively. The dimensionless parameter involving the Young's modulus is plotted in Fig. 14, and has been evaluated according to Eq. (22). The effect of Young's modulus increases with increasing the confining pressure. The effect of confining pressure on the initial response can be explained analysing influence of the confining pressure on the coordination number shown in Fig. 16. The higher the confining pressure, the more compact the specimen and the greater the coordination number. According to theoretical estimation expressed by Eq. (22) the Young's modulus is proportional to the coordination number. The numerical estimations of the Young's modulus are closer to the theoretical values for higher values of the confining pressure. This is another evidence that the theoretical estimations based on the Voigt's hypothesis are more accurate for more compact granular materials that was remarked above.

5. Conclusions

The numerical studies performed in this work have confirmed that the complex behaviour of granular material can be reproduced with a discrete element model employing spherical particles. The results of simulations of the triaxial compression tests have allowed to determine the relationships between the macroscopic elastic moduli (the Young's, bulk and shear moduli and Poisson's ratio) and the basic parameters of the interparticle contact model (the contact stiffness in the normal and tangential direction and the Coulomb friction coefficient). The results can be used in calibration of discrete element models. Although the use of the simple contact model, without moment interactions, imposes the limits on the range of macroscopic parameters, it allows to better understand an influence of the investigated model parameters on macroscopic response. The numerical results have been compared with analytical estimations based on the kinematic Voigt's hypothesis. It has been shown that numerical results are close to theoretical predictions for particle assemblies with higher coordination numbers. Higher coordination numbers are related to more compact specimens. For a given specimen coordination numbers can be associated with the low values of contact stiffness and higher confining pressure.

The results have also shown that the analytical formulae gives good solutions for the particle assemblies in which overall deformation is governed by the elastic deformation at the contact, with no or small influence of particle rearrangement. This is also associated with lower values of the contact stiffness that allows bigger particle overlaps. For higher values

of the contact stiffness, its effect on the initial macroscopic response is very small, since then, the particle penetrations play a minor role, with respect to interparticle sliding and rearrangement.

The numerical results obtained for a wide range of the contact stiffness constitute a bridge between the range of the low values of the contact stiffness in which the analytical estimations are valid and the range in which the analytical and numerical results diverge. It shows the range of validity of theoretical predictions – the theoretical formulations should give a reasonably good estimations of the initial moduli for ''soft'' granular materials characterized with low macroscopic stiffness. Calibration of DEM models for ''hard'' granular materials such as sands should be based on numerical simulation since the numerical results diverge a lot from the theoretical predictions.

In our analysis, we have introduced original dimensionless numbers different from those used in other works [23,28]. Thanks to incorporation of micromechanical parameters such as coordination number and porosity to the dimensionless parameter we create a common framework to analyse properties of different specimens.

The studies in the present work have not accounted for the effect of porosity on the elastic moduli. Depending on the porosity granular materials can have quite different behaviour. It is observed in experimental tests [40], as well as in numerical simulation [2]. The DEM is a suitable tool to investigate an influence of the porosity on the macroscopic properties and flow of the granular material. By averaging particles volume within appropriately chosen representative volume elements it is possible to obtain porosity fields within the volume occupied by a granular material [7]. Due to its importance and complexity, the effect of porosity deserves a special and comprehensive study, such as the one for cohesive materials, that has been carried out in [43].

Acknowledgements

The work presented in this paper has been partially funded by the Polish National Science Centre within a project awarded by decision number DEC-2013/11/B/ST8/03287.

REFERENCES

[1] P. Cundall, O. Strack, A discrete numerical method for granular assemblies, Geotechnique 29 (1979) 47–65.
[2] L. Widuliński, J. Kozicki, J. Tejchman, Numerical simulations of triaxial test with sand using DEM, Archives of Hydro-Engineering and Environmental Mechanics 56 (2009) 149–171.
[3] J. Plassiard, N. Belheine, F. Donze, A spherical discrete element model: calibration procedure and incremental response, Granular Matter 11 (2009) 293–306.
[4] V. Murthy, Geotechnical Engineering: Principles and Practices of Soil Mechanics and Foundation Engineering, CRC Press, 2002.
[5] L. Wu, F. Qu, Discrete element simulation of mechanical characteristic of conditioned sands in earth pressure balance shield tunneling, Journal of Central South University of Technology 16 (2009) 1028–1033.
[6] R. Balevičius, I. Sielamowicz, Z. Mróz, R. Kačianauskas, Effect of rolling friction on wall pressure, discharge velocity and outflow of granular material from a flat-bottomed bin, Particuology 10 (2012) 672–682.
[7] I. Sielamowicz, R. Balevičius, Experimental and computational analysis of granular material flow in model silos, IFTR Reports on Fundamental Technological Research (1/2012), 2012.
[8] C. Martin, D. Bouvard, S. Shima, Study of particle rearrangement during powder compaction by the Discrete Element Method, Journal of the Mechanics and Physics of Solids 51 (2003) 667–693.
[9] J. Rojek, F. Zarate, C.A. de Saracibar, C. Gilbourne, P. Verdot, Discrete element modelling and simulation of sand mould manufacture for the lost foam process, International Journal for Numerical Methods in Engineering 62 (2005) 1421–1441.
[10] J. Rojek, E. Oñate, C. Labra, H. Kargl, Discrete element simulation of rock cutting, International Journal of Rock Mechanics and Mining Sciences 48 (2011) 996–1010.
[11] D. Potyondy, P. Cundall, A bonded-particle model for rock, International Journal of Rock Mechanics and Mining Sciences 41 (2004) 1329–1364.
[12] T. Wu, I. Temizer, P. Wriggers, Computational thermal homogenization of concrete, Cement and Concrete Composites 35 (2013) 59–70.
[13] L. Rothenburg, R.J. Bathurst, Micromechanical features of granular materials with planar elliptical particles, Geotechnique 42 (1) (1992) 79–95.
[14] H. Tao, W. Zhong, B. Jin, Flow behavior of non-spherical particle flowing in hopper, Frontiers in Energy 3 (2014) 315–321.
[15] P. Digby, The effective elastic moduli of porous granular rocks, Journal of Applied Mechanics 48 (1981) 803–808.
[16] K. Walton, The effective elastic moduli of a random packing of spheres, Journal of Mechanics and Physics of Solids 35 (1987) 213–226.
[17] R. Bathurst, L. Rothenburg, Micromechanical aspects of isotropic granular assemblies with linear contact interactions, ASME Journal of Applied Mechanics 55 (1988) 17–23.
[18] C. Chang, Micromechanical modelling of constitutive equation for granular material, in: J. Jenkins, M. Satake (Eds.), Micromechanics of Granular Materials, Elsevier Science Publishers, 1988 271–278.
[19] C. Liao, T. Chang, D. Young, Stress–strain relationship for granular materials based on the hypothesis of best fit, International Journal of Solids and Structures 34 (1997) 4087–4100.
[20] C. Chang, S. Chao, Y. Chan, Estimates of elastic moduli for granular material with anisotropic random packing structure, International Journal of Solids and Structures 32 (14) (1995) 1989–2008.
[21] J. Jenkins, D. Johnson, L.L. Ragione, H. Makse, Fluctuations and the effective moduli of an isotropic, random aggregate of identical, frictionless spheres, Journal of the Mechanics and Physics of Solids 53 (2005) 197–225.
[22] S. Luding, Micro–macro transition for anisotropic, aperiodic, granular materials, International Journal of Solids and Structures 41 (2004) 5821–5836.
[23] N. Kruyt, I. Agnolin, S. Luding, L. Rothenburg, Micromechanical study of elastic moduli of loose granular materials, Journal of the Mechanics and Physics of Solids 58 (2010) 1286–1301.
[24] C. Guan, J. Qi, N. Qiu, G. Zhao, Q. Yang, X. Bai, C. Wang, Macroscopic Young's elastic modulus model of particle packing rock layers, Open Journal of Geology 2 (2012) 198–202.
[25] C. Chang, Constitutive modeling for granular material under finite strains with particle slidings and fabric changes, Tech. rep. Final Report on Research under Grant No. AFOSR

89-0313, Department of Civil Engineering, University of Massachusetts, 1992.
[26] I. Agnolin, J. Roux, Internal states of model isotropic granular packings. III. Elastic properties, Physical Review E 76 (2007) 061304.
[27] I. Agnolin, N. Kruyt, On the elastic moduli of two-dimensional assemblies of disks: relevance and modeling of fluctuations in particle displacements and rotations, Computers and Mathematics with Applications 55 (2008) 245–256.
[28] H. Makse, N. Gland, D. Johnson, L. Schwartz, Why effective medium theory fails in granular materials, Physical Review Letters 83 (1999) 5070–5073.
[29] J. Ma, I. Temizer, P. Wriggers, Random homogenization analysis in linear elasticity based on analytical bounds and estimates, International Journal of Solids and Structures 48 (2011) 280–291.
[30] C. Coetzee, D. Els, Calibration of discrete element parameters and the modeling of silo discharge and bucket filling, Computers and Electronics in Agriculture 65 (2009) 198–212.
[31] Y. Yan, S. Ji, Discrete element modeling of direct shear tests for a granular material, International Journal for Numerical and Analytical Methods in Geomechanics 34 (2010) 978–990.
[32] R. Kačianauskas, A. Maknickas, A. Kačeniauskas, D. Markauskas, R. Balevičius, Parallel discrete element simulation of poly-dispersed granular material, Advances in Engineering Software 41 (2010) 52–63.
[33] J. Kozicki, J. Tejchman, Z. Mróz, Effect of grain roughness on strength, volume changes, elastic and dissipated energies during quasi-static homogeneous triaxial compression using DEM, Granular Matter 14 (2012) 457–468.
[34] F. Calvetti, G. Viggiani, C. Tamagnini, A numerical investigation of the incremental behavior of granular material soils, Rivista Italiana di Geotecnica 3 (2003) 11–29.
[35] CIMNE, Dempack: explicit nonlinear dynamic analysis by the finite and discrete element method. Available at: www.cimne.upc.edu/dempack.
[36] E. Oñate, J. Rojek, Combination of discrete element and finite element methods for dynamic analysis of geomechanics problems, Computer Methods in Applied Mechanics and Engineering 193 (2004) 3087–3128.
[37] J. Rojek, C. Labra, O. Su, E. Oñate, Comparative study of different discrete element models and evaluation of equivalent micromechanical parameters, International Journal of Solids and Structures 49 (2012) 1497–1517.
[38] E. Kuhl, G.A. D'Addetta, H.J. Herrmann, E. Ramm, A comparison of discrete granular material models with continuous microplane formulations, Granular Matter 2 (2000) 113–121.
[39] C. Labra, E. Oñate, High density sphere packing for discrete element method simulations, Communications in Numerical Methods in Engineering 25 (7) (2009) 837–849.
[40] Y. Wan, Discrete element method in granular material simulations, Institute of Fraunhofer ITWM Kaiserslautern/Technical University of Kaiserslautern, 2011 (Ph.D. thesis).
[41] S. Mesarovic, J. Padbidri, B. Muhunthan, Micromechanics of dilatancy and critical state in granular matter, Geótechnique Letters 2 (2012) 61–66.
[42] S. Antony, N. Kruyt, Role of interparticle friction and particle-scale elasticity in the shear-strength mechanism of three-dimensional granular media, Physical Review E 79 (2009) 031308.
[43] M. Schopfer, S. Abe, C. Childs, J.J. Walsh, The impact of porosity and crack density on the elasticity, strength and friction of cohesive granular materials: insights from DEM modeling, International Journal of Rock Mechanics and Mining Sciences 46 (2009) 250–261.